Metal-Insulator Transition in $(V_{1-x}Cr_x)_2O_3$

D. B. McWhan and J. P. Remeika
Bell Telephone Laboratories, Murray Hill, New Jersey 07974
(Received 24 April 1970)

A first-order metal-insulator transition with no change in long-range order occurs in the mixed oxides $(V_{1-x}Cr_x)_2O_3$ with increasing x ($x \approx 0.01$ at 1 atm and 298 °K) or decreasing pressure (at ≈ 10 kbar for $x = 0.04$ at 298 °K). In a preliminary letter it was shown that the transition had all the qualitative features expected of a Mott transition, i.e., a transition from band to localized behavior. The present paper reports the detailed experimental results. Single crystals of mixed oxides have been made by reaction of Cr_2O_3, V_2O_5, and VN in molten KF. Electrical resistivity and powder x-ray diffraction measurements made as a function of temperature and pressure in oxides with $0 \leq x \leq 0.12$ establish a temperature-pressure-composition phase diagram with three clearly defined phases: metal (M), insulator (I), and antiferromagnetic insulator (AF). The I-M transition is marked by a drop of over two orders of magnitude in the electrical resistivity and a discontinuous decrease in volume of $\approx 1.2\%$ with no change in crystal structure. For $x \approx 0.01$ the sequence AF → M → I is observed with increasing temperature at 1 atm. At 4.2 K an AF → M transition occurs with increasing pressure ($P = 41 \pm 6$ kbar for $x = 0.04$). The phase diagram is compared with other transition-metal oxides, and the differences between the transition in V_2O_3 and VO_2 are discussed.

INTRODUCTION

It has been known since the 1930's that there are two classes of solids.[1] One class can be described using Bloch-Wilson band theory, and the second class, consisting of magnetic insulators, can be described using a localized or Heitler-London approach. These two classes are qualitatively different in the nature of the wave functions used to describe them. The transition from the band class to the localized class does not require a change in long-range order, and it is of interest to determine the nature of this transition. In 1949, Mott argued that the long-range Coulomb interaction would cause the transition to be discontinuous as a function of volume.[2] In a subsequent paper, Mott proposed a phase diagram for a first-order transition between a degenerate electron gas and a localized antiferromagnetic insulator at low temperatures.[3] The qualitative idea of such a sharp, possibly first-order transition in the nature of the electronic wave function is often called a Mott transition. Since that time serious questions have arisen about the possibility of observing a Mott transition and about being able to identify the actual driving mechanism in metal-insulator transitions. A discussion of these problems can be found in Ref. 4.

There are metal-insulator transitions which are clearly not related to the Mott transition. For example, materials such as Si and Ge have first-order insulator-metal transitions with increasing pressure.[5] However, these transitions are associated with a change in crystal structure and both the insulating and metallic phases are describable by band theory. Another type of transition which has been discussed theoretically results from a change in band overlap without a structure change. If two bands either cross or uncross as a function of an external variable such as pressure, then in a pure system a metal-insulator transition will occur. In this case the weak coupling theory for the Coulomb interaction between electrons and holes predicts the existence of an occluded excitonic phase between the metal and the insulator at low temperature.[6] There are several materials such as Yb and Bi in which a band uncrossing does occur with increasing pressure. However, no evidence for an excitonic phase has been found.[7,8]

Attempts to find examples of a Mott transition in crystalline solids have not been too successful. For example, pressures of 400 kbar have not produced a transition to a metallic state in NiO.[9] Disordered systems such as doped semiconductors do show continuous changes from insulating to metallic conductivity as a function of doping. These are related to a Mott transition and are believed to be associated with a change from localized to band impurity states.[2,4]

In 1946 Föex found that V_2O_3 has a sharp temperature-induced insulator-metal transition.[10] A similar transition was also found in VO_2,[11] and these results were confirmed using single-crystal samples by Morin.[12,13] In each case there are lattice distortions associated with the insulating phase. In addition, V_2O_3 is antiferromagnetic below the transition.[14-16] These complications make it difficult to tell if the principal driving force in these transitions is of the type suggested by Mott. Since V_2O_3 is metallic at room temperature but Cr_2O_3 is insulating, it is reasonable to ask how the metal-insulator

transition will occur in the mixed oxide system $(V_{1-x}Cr_x)_2O_3$. Unpublished x-ray diffraction studies of this system show that there is a smooth variation in the volume and the c/a ratio of the lattice parameters as x varies from 1.0 to 0.02.[17] However, pure V_2O_3 is markedly different. Also the addition of small amounts of Cr_2O_3 to V_2O_3 results in a rapid increase in the resistivity.[18] These studies suggest that there is an anomalous region in the mixed oxide system at the V-rich end.

In a preliminary paper[19] the existence of a first-order insulator-metal transition, with no change in crystal structure, was established in the $(V_{1-x}Cr_x)_2O_3$ system, both with increasing pressure and decreasing Cr concentration. It was shown that this transition has all the qualitative features of a Mott transition and that it was difficult to explain on other grounds. A more detailed comparison with the different theories for the metal-insulator transition has been given elsewhere.[20]

The present paper reports the detailed experimental results, and it is divided into four sections. In Sec. I the preparation and characterization of single-crystal samples of the different mixed oxides is discussed. X-ray diffraction studies and electrical resistivity measurements are presented in Secs. II and III. The different experiments were designed to establish the general features of a pressure-temperature-composition phase diagram for the $(V_{1-x}Cr_x)_2O_3$ system. Three regions are clearly separable: metal (M), paramagnetic insulator (I), and antiferromagnetic insulator (AF). The electrical and crystallographic properties of each region are markedly different, and the different phase boundaries can be detected independently by the x-ray and resistivity measurements. In Sec. II the structural properties of each region are determined by powder x-ray diffraction measurements. The AF-M, AF-I, and M-I transitions are established as a function of temperature for several different compositions. The I-M transition was determined as a function of pressure at room temperature for a sample with 4% Cr. In addition, the compressibility of V_2O_3 was determined. In Sec. III resistivity measurements were used to determine independently the M-I transition at room temperature as a function of composition. Next, the AF-M, AF-I and M-I transitions were determined by resistivity-versus-temperature measurements. Finally, measurements at high pressures were used to establish the pressure-temperature phase diagram for $(V_{0.96}Cr_{0.04})_2O_3$. In Sec. IV the data are used to construct a three-dimensional pressure-temperature-composition phase diagram. This diagram is discussed in the context of transition-metal oxides in general, and it is suggested that M-I boundaries exist in the monoxides, sesquioxides, and dioxides. Finally, some of the differences between the temperature-induced transitions in V_2O_3 and VO_2 are discussed. In the Appendix, a temperature-volume phase diagram for $(V_{0.96}Cr_{0.04})_2O_3$ is constructed to show the volume excluded in the different transitions.

In conjunction with the present work, a series of related studies have been carried out on the metal-insulator transition. In order to present as comprehensive a picture as possible the results are being published together as a series of six papers of which this is the first. The second paper reports measurements which establish that the metal-insulator phase boundary terminates at a solid-solid critical point for a given Cr concentration.[21] The third reports the magnetic susceptibility as a function of temperature and Cr concentration.[22] The fourth gives the results of NMR experiments on V_2O_3 which were performed at 4.2 °K as a function of pressure up to ≈ 65 kbar.[23] The fifth reports measurement of the nuclear specific heat of V_2O_3 at low temperatures.[24] In the sixth paper a refinement of the crystal structure of the AF phase of V_2O_3 is presented.[25] In a separate paper, Brinkman and Rice present calculations on the Hubbard model and discuss the role of Hund's-rule energies in the metal-insulator transition.[26]

I. PREPARATION AND CHARACTERIZATION OF CRYSTALS OF V_2O_3 AND $(V_{1-x}Cr_x)_2O_3$

V_2O_3 is usually prepared in powdered form by heating mixtures of $V_2O_5 + V$ in sealed tubes or by the reduction of V_2O_5 by H_2. Most of the measurements reported in the literature on single-crystal samples were made on crystals grown by the technique of flame fusion, from a melt of V_2O_5 in a controlled reducing atmosphere, or by hydrothermal methods. Stoichiometry is difficult to control in these syntheses. In an attempt to overcome this problem a series of experiments were performed to test the feasibility of growing crystals out of solution at high temperatures. Attempts to use VF_3 as a flux and grow crystals of V_2O_3 by solution of V_2O_3 in molten VF_3 under a protective atmosphere of Ar were unsuccessful. Sublimation of the VF_3 could not be controlled.

Another high-temperature solvent was then sought and KF was chosen on the basis of its convenient melting point, its limited reaction with the nutrient materials, and its high solubility in cold water (a necessary prerequisite for crystal extraction). It was also believed that potassium would be excluded from the lattice of V_2O_3 because of its large size. The envisioned reaction required a room-temperature stable compound of vanadium that would then react with V_2O_5 at elevated temperatures to form V_2O_3. The V_2O_3 was expected to be transported through the molten KF and subsequently crystallized by nucleation and growth at the cooler regions in the crucible. VN was selected as the vanadium reactant, and it is

believed the reaction proceeds as follows:

$$2VN + 3V_2O_5 \xrightarrow[KF]{950\,^\circ C} 4V_2O_3 + 2NO_x \uparrow.$$

In practice, we found it necessary to use an excess of V_2O_5 above that required for the reaction with VN to produce V_2O_3. Some reaction with KF does seem to occur, producing a transparent green product which is slightly less soluble in H_2O than KF. We did not identify the green product, although we presume it to be a potassium vanadium oxyfluoride. A typical run was made by weighing the following components (in grams) into a 100-cm^3 platinum crucible. VN = 1.25, V_2O_5 = 7.50, and KF = 90.0. The crucible is placed in an atmosphere controlled tube furnace, flushed with Ar, then with a small argon flow the furnace is heated to 950 °C. This temperature is maintained for a period of 72 h. The furnace power is then turned off and the system allowed to cool to room temperature maintaining the Ar flow. The crucible is immersed in cold distilled H_2O, whereupon the flux is rapidly dissolved, leaving the crystals of V_2O_3. We found that single-crystal V_2O_3 prepared by this method dissolved extensively when kept in boiling H_2O for a period of hours. Well-faceted rhombohedral prisms of V_2O_5 ≈5 mm across and 1 mm thick could be prepared in this way. The mixed oxides were prepared by adding Cr_2O_3 to the mixture. A distribution coefficient of ≈ 2.8 was calculated for the ratio of Cr to Cr plus V in the crystals divided by the ratio in the starting mixture. The size of the crystals in the mixed oxides decreases rapidly with increasing Cr content, and the crystals are less than 0.1 mm for $(V_{0.88}Cr_{0.12})_2O_3$.

The main problem with this technique of crystal growth is that the resulting crystals contain small amounts of occluded VN. The VN is observed both in x-ray diffraction powder patterns and in ^{51}V NMR.[27] (At low temperatures the resonance from V_2O_3 is shifted to much higher frequencies by the magnetic ordering, but a resonance corresponding to VN is still observed.) By increasing the temperature of the crystal growth, the amount of occluded VN is reduced so that it is no longer detected by x-ray diffraction methods but it is still observed by NMR techniques. However, the size of the resulting crystals also decreases with increasing temperature and the growth temperature of 950° C represents a compromise between crystal size and VN content.

Attempts to obtain reliable analyses of the crystals have not been completely successful. Typical analyses by atomic absorption and emission spectrographic techniques in weight percent are vanadium 68.3%, oxygen 30.9%, and nitrogen 1.0%. Stoichiometric V_2O_3 would be vanadium 67.8% and oxygen 32.2%. Because of the presence of VN as a second phase, it is not clear what the stoichiometry of the oxide is. If all the nitrogen formed stoichiometric VN, then the oxide would be $V_2O_{3.05}$. If there are vacancies in the VN as are always found, for example, in VO_x where $0.75 < x < 1.30$,[28] then the vanadium-to-oxygen ratio would be more or less than 2:3.05. The over-all cation-impurity content, as determined by emission spectrographic analysis, is less than 10 ppm. Since the crystals are of high purity and since they were all prepared under similar conditions, a comparison between the properties of crystals with different Cr concentrations is considered justified.

In addition to analysis of the Cr content, the mixed oxides were characterized by powder x-ray diffraction methods. At room temperature all the samples showed powder patterns compatible with the α corundum structure. The lattice parameters of the hexagonal unit cell were determined from a least-squares refinement of the high-angle x-ray diffraction data obtained from crushed crystals using Cr $K\alpha$ radiation and standard Norelco 114.6-mm powder cameras. The results are plotted as a function of Cr concentration x for $(V_{1-x}Cr_x)_2O_3$ in Fig. 1. The earlier measurements on ceramic samples are shown for comparison.[17] A two-phase region exists

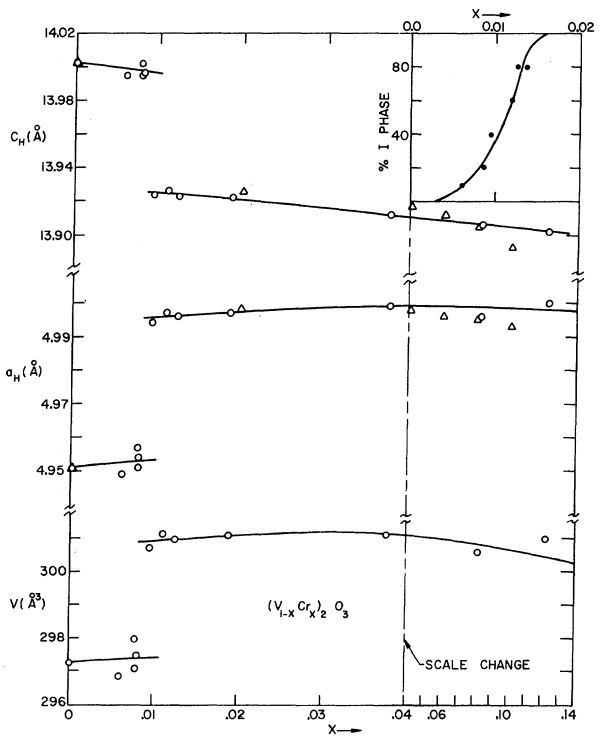

FIG. 1. Lattice parameters and volume of hexagonal cell versus Cr concentration at room temperature. Circles are this work and triangles are from Ref. 17. Inset shows fraction of expanded corundum structure (I) versus Cr as estimated from x-ray diffraction powder patterns.

near $x \approx 0.01$ between two corundum structures of different density. The ratio of the two phases was estimated from the powder films and it is plotted as the percentage of the lower density or I (insulating) phase versus x in the inset in Fig. 1. The two-phase region suggests the possibility of differences in Cr content in a given batch of crystals. However, resistivity measurements reported below show a broadening of the different transitions as a function of temperature and pressure with repeated cycling. This suggests that sample strains may be more important than concentration fluctuations, but this is by no means clear.

II. X-RAY DIFFRACTION MEASUREMENTS

A. Crystal Structure of Low-Temperature Phase V_2O_3

V_2O_3 has the trigonal α-corundum structure at room temperature but distorts to a monoclinic one at 150–160 °K. The x-ray diffraction data were originally interpreted in terms of a monoclinic distortion of an orthohexagonal cell[29]; subsequently a c-centered monoclinic cell was suggested.[30] Examination of the corundum structure shows that the correct conventional monoclinic cell is obtained from the hexagonal by the matrix

$$\begin{pmatrix} \vec{a}_M \\ \vec{b}_M \\ \vec{c}_M \end{pmatrix} = \begin{pmatrix} \frac{2}{3} & \frac{4}{3} & \frac{1}{3} \\ 1 & 0 & 0 \\ \frac{1}{3} & \frac{2}{3} & -\frac{1}{3} \end{pmatrix} \begin{pmatrix} \vec{a}_H \\ \vec{a}_H \\ \vec{c}_H \end{pmatrix}.$$

The most symmetrical space group corresponding to this cell is $I\,2/a$ (space group No. 15[31]). Positional parameters for the distorted structure are generated from the corundum structure as follows:

α corundum $R\bar{3}c$

$$\mathrm{V}(12c): \pm(00u;\ 0, 0,\ u+\tfrac{1}{2}) + rh,$$

$$\mathrm{O}(18e): \pm(v, 0,\ \tfrac{1}{4};\ 0, v, \tfrac{1}{4};\ \bar{v}, \bar{v}, \tfrac{1}{4}) + rh,$$

distorted structure $I\,2/a$

$$\mathrm{V}(8f): \pm(x, y, z;\ \tfrac{1}{2} - x, y, \bar{z}) + bc,$$

$$\text{with } x = u,\quad y \approx 0,\quad z \approx -2u$$

$$\mathrm{O}(8f):\ x \simeq \tfrac{1}{4} + v/2,\quad y \approx -v/2,\quad z \approx \tfrac{1}{2} + v/2,$$

$$\mathrm{O}(4e): \pm(\tfrac{1}{4}, y, 0) + bc,\ y \simeq \tfrac{1}{2} - v\ .$$

Using the positional parameters for the corundum structure the powder pattern for the monoclinic phase was generated, and this was used to index the powder pattern of the low-temperature phase. Powder x-ray diffraction data were obtained at 77 °K using filtered Cu K radiation and a Materials Research Corp. cryostat attachment for a General Electric diffractometer. The lattice parameters, obtained from a least-squares refinement using the resolvable high-angle reflections, are

$$a_M = 7.255 \pm 0.003\ \text{Å},\ b_M = 5.002 \pm 0.002\ \text{Å},$$

$$c_M = 5.548 \pm 0.002\ \text{Å},\ \beta = (96.75 \pm 0.02)^\circ,$$

The observed and calculated d spacings are listed in Fig. 2 and the orientation of the monoclinic unit cell is compared with that of the corundum structure in Fig. 3.

The nature of the distortion was confirmed by taking precession photographs of a single crystal which was mounted with $\vec{a}^*$ as the spindle axis. The crystal was cooled by blowing nitrogen gas of the appropriate temperature over it. Photographs of the $0kl$, $hk0$, $hk2$, and $hk4$ layers of the reciprocal lattice were recorded using Mo K radiation and Polaroid film. The spots in the $hk0$ layer only broadened on cooling through the transition, and comparison with films taken 10 °K above the transition showed that both reciprocal axes were $\approx 0.9\%$ smaller in the low-temperature phase. In the $hk2$ and $hk4$ layers each spot split to form an equilateral triangle which was oriented with the corners in the $\vec{a}^*$ directions. In the $0kl$ projection each lattice row parallel to $\vec{c}^*$ split to form an X (with single spots on one diagonal and multiple spots on the other), and $\vec{c}^*$ was $\approx 0.2\%$ larger in the distorted phase. A model compatible with the precession data is one in which the basal plane tilts with respect to the $\vec{c}$ axis. As the distortion could equally well occur in any of the equivalent directions perpendicular to the $\bar{3}$ axis, the $hk2$ and $hk4$ layers show spots corresponding to each possible $\vec{c}^*$ axis. The monoclinic angle can be determined from the size of the triangle and also from the $0kl$ layer. The parameters calculated from the single-crystal data ($a = 7.28$, $b = 4.98$, $c = 5.55$, and $\beta = 96.7^\circ$) are in agreement with the more accurate results given above and they confirm the unit cell. The expansion of the lattice and the tilting of the basal plane with respect to the corundum structure is shown in Fig. 3.

A preliminary least-squares refinement of the positional parameters was made using the powder data. The observed and calculated intensities with $I_{\mathrm{calc}} \geq 1$ are given in Fig. 2. Recently, a refinement using single-crystal data has been done and it is reported in Ref. 25.

What appears to be a strong piezoelectric response is observed on single crystals of V_2O_3 and $(V_{0.96}Cr_{0.04})_2O_3$ in the low-temperature phase using a Geibbe-Schiebe apparatus. The intensity of the piezoelectric signal decreases smoothly to below the limit of detection at ≈ 100 °K. If this represents a continuous transition to a nonpiezoelectric phase then the space group at 77 °K could still be centric ($I2/a$).

B. Variation of Lattice Parameters with Temperature

Powder x-ray diffraction measurements were

made as a function of temperature on samples of $(V_{1-x}Cr_x)_2O_3$ with $x = 0, 0.01, 0.04$. Comparison with Fig. 1 shows that these samples lie on each side of the discontinuity in the lattice parameters at room temperature and as close to the discontinuity as possible. In addition to determining the volume change at the corundum-to-monoclinic transition and the coefficients of expansion in each phase, a region of anomalous change was found at high temperatures in V_2O_3, and a temperature-induced transition similar to that observed with composition was found in the sample with $x = 0.01$.

The x-ray measurements on the samples with $x = 0$ and 0.04 were made using the Materials Research Corp. low- and high-temperature attachments for a General Electric diffractometer. For pure V_2O_3, several diffraction angles were scanned sequentially as the sample drifted up from 170 °K to room temperature using Cr $K\alpha$ radiation (214 and 300 reflections) and Cu $K\alpha$ radiation (054; 300; and 02, 16 reflections). The diffraction-angle variations with temperature were fitted to straight lines, and the resulting average coefficients of thermal expansion were $\alpha_a = 20.4$ and 19.9×10^{-6} and $\alpha_c = -8.9$ and -8.3×10^{-6} using Cr and Cu radiation, respectively. The average coefficients for V_2O_3 at 25 °C are

$$\alpha_a = \frac{1}{a}\left(\frac{da}{dT}\right) = (20.2 \pm 0.3) \times 10^{-6}\ ^\circ\mathrm{K}^{-1},$$

$$\alpha_c = \frac{1}{c}\left(\frac{dc}{dT}\right) = (-8.6 \pm 0.3) \times 10^{-6}\ ^\circ\mathrm{K}^{-1}.$$

These are in reasonable agreement with the literature values of $\alpha_a = 22 \times 10^{-6}$ and $\alpha_c = -5.8 \times 10^{-6}$.[29] No shift of the diffraction angles with temperature was detected in the monoclinic phase from 77 to 160 °K. This sets an upper limit on the coefficient of thermal expansion in the low-temperature phase of $< 2 \times 10^{-6}\ ^\circ\mathrm{K}^{-1}$.

hkl_{Hex}	hkl_{Mono}	d_{obs}	d_{calc}	I_{obs}	I_{calc}
101	110		4.109		4.4
012	011	3.703	3.703	81.0	87.2
	200	3.609	3.602	46.4	51.2
104	002	2.756	2.755	80.5	96.4
	$\bar{2}11$	2.693	2.691	100.0	126.4
110	020	2.491	2.501	178.0	67.5
	211		2.486		115.3
006	$\bar{2}02$	2.325	2.324	7.5	9.2
113	112	2.221	2.220	25.5	20.4
	$\bar{1}21$	2.204	2.202	26.6	25.7
	310	2.168	2.165	17.5	18.8
021	121	2.133	2.142	1.4	3.2
202	202	2.089	2.074	*	1.5
	220	2.055	2.054	*	6.2
024	022	1.852	1.852	77.2	69.3
	400	1.805	1.801	16.0	23.0
116	013	1.725	1.724	68.3	58.9
	$\bar{2}22$	1.706	1.702	54.0	54.9
	$\bar{4}11$	1.675	1.673	43.3	61.2
018	$\bar{2}13$	1.626	1.627	5.0	6.3
211	321		1.614		2.7
	$\bar{4}02$		1.596		2.1
	222	1.597	1.596	5.8	0.5
122	031		1.596		2.8
	$\bar{4}11$	1.573	1.572	4.3	8.0
	213	1.492	1.492	33.0	24.4
214	$\bar{2}31$	1.479	1.478	18.5	22.5
	420	1.463	1.462	16.3	21.4
300	231	1.439	1.441	74.7	49.4
	402		1.432		27.4
125	$\bar{1}32$	1.419	1.416	1.8	3.5
208	004	1.377	1.377	0.8	1.8
	$\bar{2}04$	1.341	1.340	6.8	10.6
10,10	$\bar{1}14$	1.334	1.333	2.7	3.2
	$\bar{4}13$	1.321	1.320	13.4	24.5
119	$\bar{3}23$	1.317	1.317	4.4	1.0
	$\bar{5}12$	1.300	1.297	2.4	2.5
220	040	1.251	1.251	4.8	5.3

hkl_{Hex}	hkl_{Mono}	d_{obs}	d_{calc}	I_{obs}	I_{calc}
220	422	1.245	1.243	10.1	11.1
	204		1.239		0.9
	033	1.235	1.234	4.2	3.3
306	$\bar{4}31$	1.217	1.215	1.6	4.6
223	323		1.210		1.9
	024	1.208	1.207	2.1	1.3
128	600		1.201		2.0
	$\bar{2}33$		1.197		1.3
223	521		1.192		1.4
	240		1.181		3.7
312	$\bar{2}24$	1.18	1.181	15.6	10.9
02,10	431		1.175		2.9
00,12	$\bar{5}04$	1.163	1.162	2.3	3.2
	602	1.153	1.151	3.7	5.2
	233	1.138	1.141	13.0	8.5
134	042		1.139		4.6
	611	1.119	1.117	2.2	3.7
	224	1.110	1.110	10.4	8.1
226	$\bar{2}42$	1.101	1.101	9.9	9.7
	620	1.084	1.082	14.0	10.7
	015	1.076	1.076	10.8	10.6
21,10	242		1.071		1.9
042	$\bar{4}33$	1.057	1.058	11.5	7.8
	602		1.056		1.8
	622	1.048	1.046	4.6	7.5
404	404	1.038	1.037	4.7	3.0
	440	1.028	1.027	2.6	1.9
318	215		1.000		2.4
321	150		0.9909		1.5
01,14	$\bar{4}15$	0.9743	0.9744	6.4	4.9
229	$\bar{3}43$		0.9731		1.0
232	622		0.9730		1.3
	604		0.9629		1.8
	424	0.9580	0.9578	12.2	8.0
324	$\bar{2}51$	0.9551	0.9546	8.5	6.7
	251	0.9446	0.9445	6.7	6.9
	631		0.9442		4.6
140	442	0.9423	0.9420	3.6	5.2

hkl_{Hex}	hkl_{Mono}	d_{obs}	d_{calc}	I_{obs}	I_{calc}
140	613	0.9382	0.9380	5.1	5.1
048	044		0.9259		2.7
	035	0.9192	0.9193	16.0	7.2
	$\bar{2}06$	0.9167	0.9160	5.6	2.2
13,10	$\bar{2}44$	0.9143	0.9143	4.6	10.6
20,14	$\bar{2}35$	0.9123	0.9124	4.8	2.1
	$\bar{5}24$	0.897	0.8986	9.7	5.7
30,2	$\bar{5}33$		0.8969		3.4
	$\bar{8}11$		0.8914		9.4
	$\bar{8}02$		0.8874		2.5
	415	0.8800	0.8804	11.3	5.4
	244		0.8801		5.7
	053	0.8784	0.8785	5.0	4.4
416	$\bar{4}51$	0.8715	0.8715	5.3	5.7
11,15	$\bar{3}25$		0.8714		1.3
238	235	0.8694	0.8705	1.4	1.3
31,11	$\bar{5}43$		0.8675		0.6
	640	0.8664	0.8661	19.0	8.2
	206	0.8652	0.8658	6.3	4.4
	$\bar{2}26$		0.8601		7.3
40,10	$\bar{4}06$	0.860	0.8600	22.2	2.9
10,16	811		0.8596		9.7
12,14	$\bar{4}35$	0.8534	0.8534	5.0	5.2
	$\bar{6}15$	0.8516	0.8514	4.2	4.8
	$\bar{4}44$		0.8512		0.3
	$\bar{5}42$	0.8475	0.8471	6.9	13.0
	253	0.8425	0.8427	7.6	8.5
	$\bar{8}13$	0.8370	0.8370	1.9	4.9
22,12	$\bar{8}22$		0.8363		1.0
054	060	0.8334	0.8337	5.6	4.7
330	633	0.8289	0.8287	14.3	13.9
	802	0.8270	0.8278	4.2	2.5
	226	0.8179	0.8182	9.8	8.1
32,10	316		0.8149		1.3
02,16	$\bar{4}26$	0.8131	0.8133	13.2	8.3
419	145		0.8133		1.5
	$\bar{4}53$	0.8079	0.8077	13.7	7.1
422	642		0.8069		3.3

*Cu 111 from holder interferes

FIG. 2. Comparison of observed and calculated powder x-ray diffraction data for the antiferromagnetic phase of V_2O_3. The splitting of the diffraction lines which result from the distortion from trigonal (hexagonal setting) to monoclinic is shown between the first two columns. The α_1 and α_2 peaks are resolved below the hexagonal 134 reflection, and the d spacings for Cu $K\alpha_1$ ($\lambda = 1.54051$ Å) are listed.

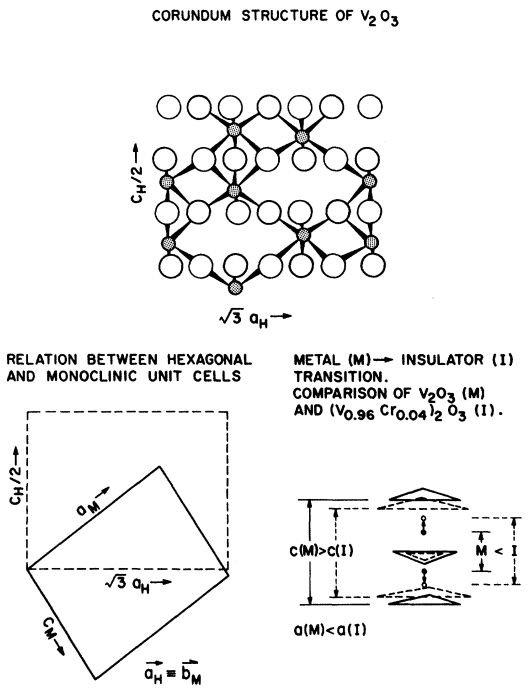

FIG. 3. Structural relations between different phases in $(V_{1-x}Cr_x)_2O_3$ system. Projection of part of the corundum structure along the hexagonal a_H axis (top). Relation of the unit cell of the low-temperature phase to that of the hexagonal unit cell (bottom left). Note the effective tilting and expansion of the basal plane which results from the monoclinic distortion. Change in interatomic distances on going from the collapsed (M) to the expanded (I) corundum structure with the addition of Cr (after Ref. 53; on bottom right). Note that c_H decreases as the V–V distance along c_H increases.

The volume of the rhombohedral unit cell just above the transition is 98.61 ± 0.05 Å^3, and the volume of the primitive monoclinic unit cell (i.e., $\frac{1}{2}$ the body-centered unit cell) is 99.97 ± 0.08 Å^3. The percent change in volume at the transition from the rhombohedral to the monoclinic phase is (1.4 ± 0.1)% which is between the literature values of 0.6[11] and 3.5.[32]

There is an anomaly in V_2O_3 between 500 and 600 °K which is marked by a rise in the resistivity and a change in the thermal expansion.[11,33] The diffraction angles for the 054; 300; 02, 16; and 32, 10 reflections were measured at different fixed temperatures up to ≈700 °K and the lattice parameters were obtained from a least-squares refinement. The results are plotted in Fig. 4. The different symbols are for data taken with increasing and decreasing temperature and on recycling through the high-temperature range. The reproducibility of the results and the lack of an anomaly in the sample with $x = 0.04$ strongly suggest that the anomaly does not result from a change in stoichiometry and that it is an intrinsic property of V_2O_3. Pseudohexagonal axes are shown for the monoclinic phase to emphasize the change at the transition. The average coefficients of expansion were used with the room-temperature lattice parameters to draw the curves from 170 to 298 °K and smooth curves were drawn through the high-temperature points.

Similar measurements were made at low and high temperatures on $(V_{0.96}Cr_{0.04})_2O_3$. The thermal expansion is much smaller as can be seen in Fig. 4. The coefficients of expansion were obtained by fitting the high-temperature data to straight lines, and the coefficients at 25 °C are

$$\alpha_a = (8.8 \pm 1.0) \times 10^{-6}\,°K^{-1},$$

$$\alpha_c = (3.5 \pm 1.0) \times 10^{-6}\,°K^{-1}.$$

The lattice parameters of the monoclinic phase of the 4% Cr sample at 77 °K are $a = 7.277 \pm 0.007$, $b = 4.997 \pm 0.005$, $c = 5.540 \pm 0.005$, and $\beta = 96.74 \pm 0.05$, and they are very similar to those of pure V_2O_3. The change in volume at the transition from the rhombohedral to the monoclinic phase is $-(0.1 \pm 0.1)$%. This is substantially smaller than the value of $+(1.4 \pm 0.1)$% found for pure V_2O_3.

Measurements on a sample of $(V_{0.99}Cr_{0.01})_2O_3$ re-

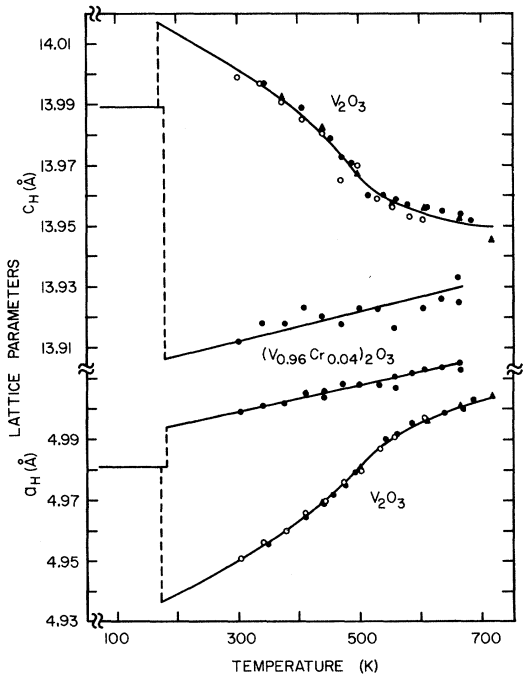

FIG. 4. Lattice parameters versus temperature for V_2O_3 and $(V_{0.96}Cr_{0.04})_2O_3$. The reproducibility of the anomaly in V_2O_3 at high temperature is shown by the solid and open circles representing the first and second heating cycles, respectively, and the triangles for the first cooling cycle. Pseudo a and c axes are shown for the monoclinic phase.

vealed a temperature-induced first-order transition with no change in crystal structure but a change in volume. At lower temperatures a second transition to the monoclinic structure (AF) occurred. In this experiment the sample was mounted on a copper disk which was suspended by three thin stainless-steel wires in a Philips diffractometer. The temperature was varied from 150 to 350 °K by blowing nitrogen gas of the appropriate temperature over the sample, and the temperature monitored with a thermocouple mounted on the back of the disk (the gradient across the disk was determined in a separate experiment). The 300 and 214 reflections were recorded using filtered Cu K radiation. The volume calculated from these reflections is compared with that calculated for V_2O_3 (M phase) and for $(V_{0.96}Cr_{0.04})_2O_3$ (I phase) in Fig. 5(a). With increasing temperature a transition occurs and the intensities of the reflections corresponding to the M phase decrease and those of the I phase increase. The hysteresis in the transition is shown in Fig. 5(b) where the fraction of the sample in the V_2O_3-like phase, $I(\mathrm{M})/[I(\mathrm{M})+I(\mathrm{I})+I(\mathrm{AF})]$, where I is the intensity of the diffraction peak, is plotted versus temperature for both cooling and warming. The broadness of the transition may reflect inhomogeneities in composition and variations in strain produced in the sample by powdering and repeated cycling through the transition. The volume change observed in the temperature-induced M-I transition is the same within experimental error as that observed as a function of composition at room temperature.

C. Variation of Lattice Parameters with Pressure

A transition between corundum structures of different density was found with changes in Cr concentration (Fig. 1) and in $(V_{0.99}Cr_{0.01})_2O_3$ as a function of temperature. Resistivity measurements reported in Sec. III show a sharp drop of over two orders of magnitude at ≈ 11 kbar in $(V_{0.96}Cr_{0.04})_2O_3$. In order to determine if this drop in resistivity is associated with the same type of transition, powder x-ray diffraction measurements were made on V_2O_3, $(V_{0.96}Cr_{0.04})_2O_3$, and Ti_2O_3 at room temperature as a function of pressure up to 50 kbar. Similar measurements on the other sesquioxides with the corundum structure have already been reported.[34] Unfortunately, the expected volume change is 1–2% and the experimental error is $\approx \frac{1}{2}\%$ so that an unambiguous result is unlikely.

The measurements were made in an opposed anvil geometry where the sample in the center of a crushable boron-filled Epoxy disk is compressed between anvils.[35] This assembly forms the center of a Debye-Scherrer camera, Mo $K\alpha$ radiation was used and the camera calibrated by comparing the diffraction pattern at a nominal applied load with a pattern calculated from the known lattice parameters at 1 atm. The lattice parameters at each pressure were obtained from a least-squares refinement using 6 to 11 observable reflections, and the results are summarized in Fig. 6. Pure V_2O_3 and Ti_2O_3 show smooth variations in lattice parameters with pressure. However, the $\vec{a}$ parameter of $(V_{0.96}Cr_{0.04})_2O_3$ starts at an intermediate value and drops to a value close to that of pure V_2O_3 with increasing pressure. The scatter in the $\vec{c}$ parameter is much worse than that in $\vec{a}$, but each run (open or closed triangles) does appear to show a rise in $\vec{c}$ associated with the drop in $\vec{a}$. The direction and magnitude of the changes are in agreement with the

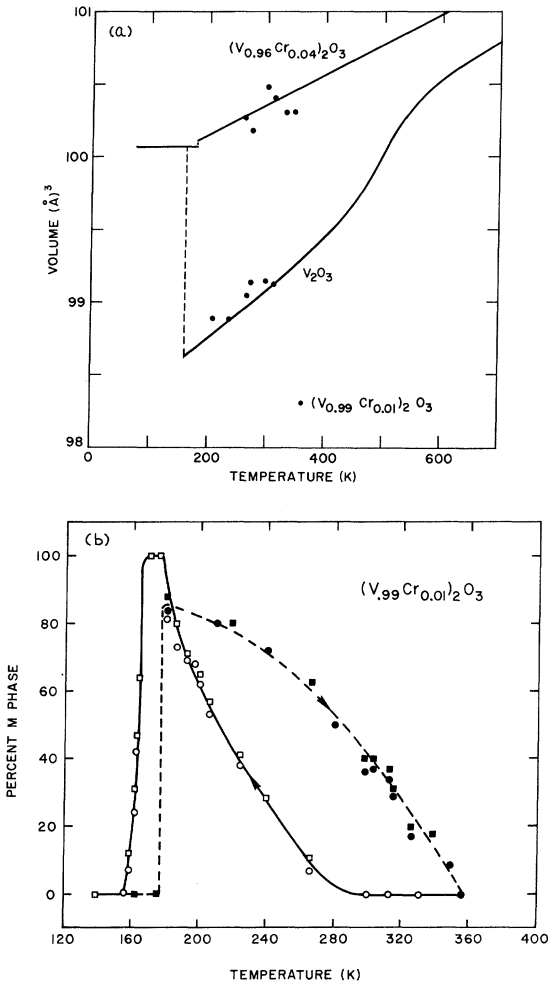

FIG. 5. Phase transitions in $(V_{0.99}Cr_{0.01})_2O_3$ as a function of temperature as determined from x-ray diffraction measurements. (a) Comparison of volume (rhombohedral cell) with that calculated from Fig. 4 for V_2O_3 and $(V_{0.96}Cr_{0.04})_2O_3$. (b) Temperature hysteresis of the transition. Percent M phase is calculated from the ratio of the peak intensities: $I(\mathrm{M})/[I(\mathrm{M})+I(\mathrm{I})+I(\mathrm{AF})]$. Squares for 214 reflection; circles for 300. Open and closed symbols for data obtained on cooling and warming, respectively.

other x-ray measurements reported in Sec. II. Thus, the transition observed in the resistivity measurements as a function of pressure is associated with a volume discontinuity but no change in crystal structure.

From the data on pure V_2O_3 and Ti_2O_3 one can calculate the volume dependence of the c/a ratio and a rough value for the bulk modulus. The pressure scale was obtained by assuming the transition in the Cr-doped sample at 11 kbar as a fixed point and by assuming a linear relation between applied load and true pressure. In one run, NaCl was added as an internal standard and this gave a maximum pressure of 63 kbar instead of the value of 47 kbar given above. However, in a mechanical mixture of NaCl and V_2O_3 both materials are not necessarily subjected to the same pressure[36,37] and, therefore, the second (NaCl) pressure calibration is less reliable.

The bulk modulus was calculated using the one-parameter Birch equation

$$P=\tfrac{3}{2}B_0\left[(V_0/V)^{7/3}-(V_0/V)^{5/3}\right],$$

where B_0 is the bulk modulus at 1 atm.[38] This equation assumes that the pressure derivative of the bulk modulus is 4, and it is known to fit a large body of P-V data. The results are

$$d\ln(c/a)/d\ln V=-0.7\ (V_2O_3)\ \text{and}\ -0.3\ (Ti_2O_3),$$

$$B_0=-dP/d\ln V=2140\pm500\ \text{kbar}\ (V_2O_3)$$

$$\text{and}\ 1860\pm500\ (Ti_2O_3).$$

The pressure calibration based on NaCl would make B_0 even larger so the error is more likely to be on the plus side. The values for B_0 given above are not unreasonable since $B_0=2505$ kbar[39] and 2027 kbar[40] for Al_2O_3 and Fe_2O_3, respectively. The values of $d\ln(c/a)/d\ln V$ can be compared with those for Cr_2O_3 (-0.3), Fe_2O_3 (0.0), and Al_2O_3 $(+0.1)$.[34] The c/a ratio is much more pressure sensitive in V_2O_3 than in any of the other sesquioxides.

III. ELECTRICAL RESISTIVITY MEASUREMENTS

A. Resistivity versus Temperature

The dc resistivity of several mixed oxides was measured from 100 to 500 °K. The samples were as-grown single-crystal rhombohedral prisms which averaged $\approx\frac{1}{2}$ mm thick (paralled to the $\vec{c}$ axis) and ≈ 2 mm across. The resistivity perpendicular to the hexagonal $\vec{c}$ axis was measured by attaching four probes to the sample with silver paste. The temperature was controlled by blowing heated or cooled nitrogen gas over a block to which the sample and an Au–0.07 at.% Fe versus Chromel thermocouple were attached with General Electric 7031 cement. The constant current used varied from 0.01 mA in the insulating phases to 10 mA in the metallic phase. The samples were heated to 500 °K and data collected on cooling at a rate of $\approx 1°$ per minute. The results depend on the sample history and are especially difficult to reproduce in the monoclinic phase. After the crystal distorts, the lead contact resistance often exceeds the samplesresistance by several orders of magnitude. The effects of cracks are also difficult to estimate so that the resistivites in the monoclinic phase are subject to errors which could be as large as a factor of 2 to 5. Average area/length ratios were measured with a filar micrometer and the resistivities are plotted as a function of Cr concentration at room temperature in Fig. 7. The estimated errors in the room-temperature resistivities are $\approx 20\%$. The size of the crystals decreases to $<\frac{1}{4}$ mm at the higher Cr concentrations so only a two-lead measurement was made for samples with $x=0.08$ and 0.12. A two-phase region was found in the x-ray diffraction studies reported in Sec. I, and this is indicated in Fig. 7. A sharp drop in resistivity is observed with decreasing Cr concentration as the percentage of the higher density co-

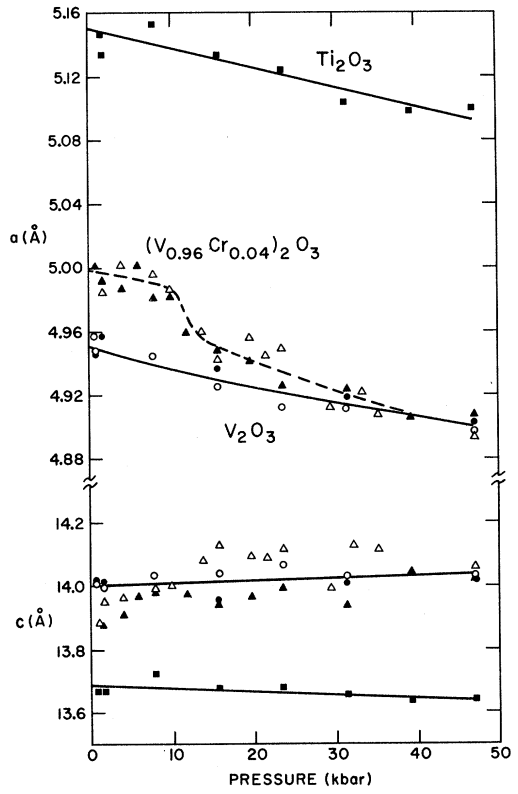

FIG. 6. Lattice parameters as a function of pressure; V_2O_3 (circles), $(V_{0.96}Cr_{0.04})_2O_3$ (triangles), and Ti_2O_3 (squares). Open and closed symbols represent different experiments. Data suggest a transition in $(V_{0.96}Cr_{0.04})_2O_3$ from a less dense to a more dense corundum phase.

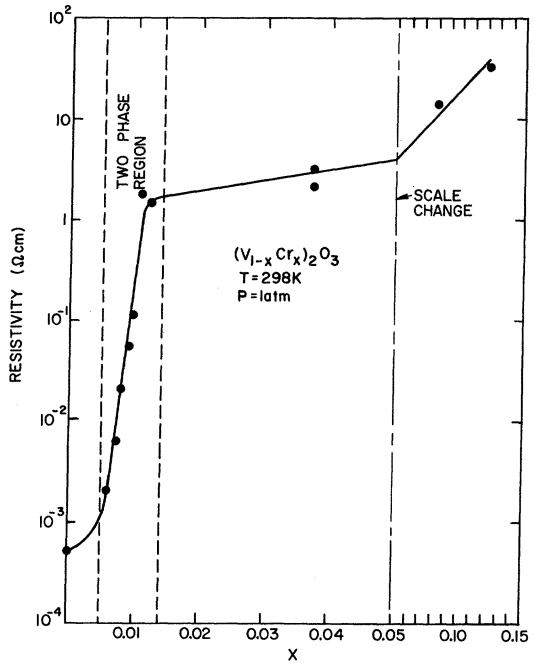

FIG. 7. Resistivity versus Cr concentration at room temperature. The two-phase region determined from x-ray diffraction patterns (Fig. 1) is shown by the dashed lines.

rundum or pure V_2O_3-like phase increases.

The results of typical resistivity–versus–reciprocal-temperature curves are shown in Fig. 8. Samples with $x > 0.01$, i.e., above the two-phase region in Fig. 7, show large negative temperature coefficients of resistivity above room temperature with an activation energy of ≈ 0.32 eV. There is a change in slope above room temperature which may reflect the onset of intrinsic behavior. The sample with $x = 0.04$ shows an anomaly on cooling at 180 °K associated with the transition to the monoclinic antiferromagnetic phase. At lower temperatures the activation energy for conduction is considerably smaller (~ 0.1 eV) than that observed at high temperature. The x-ray diffraction studies summarized in Fig. 5 show that the sample with $x = 0.01$ transforms to the higher-density corundum phase, and that a second transition to the monoclinic phase occurs at lower temperatures. As shown in Fig. 8, the transition to the high-density corundum phase is accompanied by a sharp drop in the resitivity to a value approaching that of pure V_2O_3. With repeated temperature cycling the transitions from one corundum phase to another tends to become less sharp. The transition to the monoclinic phase is qualitatively different in the sample with $x = 0.04$ from that observed in samples with $x < 0.02$. In the former case there is no observable hysteresis, and the transition is continuous. Also the sample appears to deteriorate much less on repeated temperature cycling. The hysteresis and sharpness of the transition both increase as x decreases from $0.02 \rightarrow 0.0$. Finally, it should be noted that the high-temperature anomaly in pure V_2O_3 is in the direction of approaching that of the Cr-doped samples with $x > 0.01$. In fact, the earlier work on ceramic samples shows an initial rise in resistivity near 500 °K followed by a region at higher temperatures with a negative temperature coefficient of resistivity.[8] This maximum at high temperatures was not supported by measurements on a single crystal of V_2O_3 which were reported later.[33]

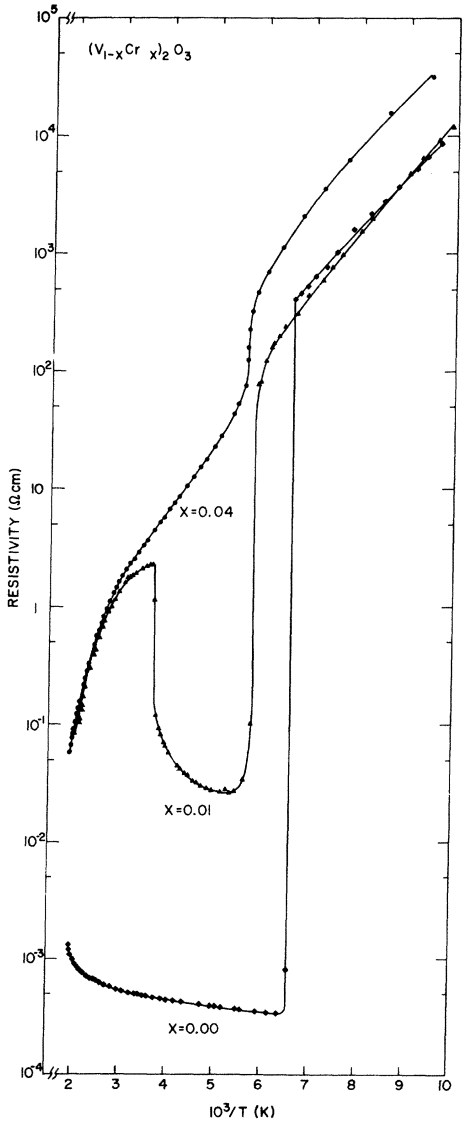

FIG. 8. Resistivity versus reciprocal temperature at 1 atm for $x = 0.00$ (diamonds), 0.01 (triangles), and 0.04 (circles).

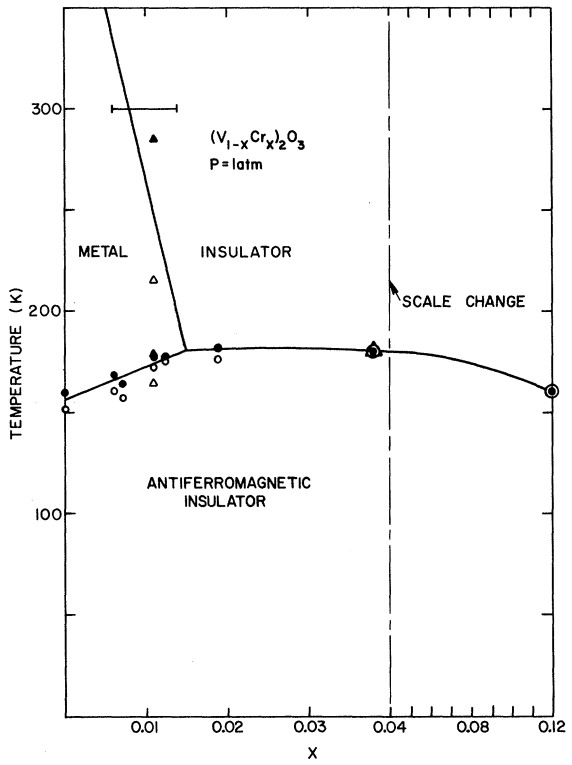

FIG. 9. Temperature-composition phase diagram at 1 atm. Closed and open circles are from resistivity measurements with increasing and decreasing temperature, respectively. Triangles are from x-ray diffraction measurements and bar shows two-phase region shown in Fig. 1.

A temperature-composition phase diagram was constructed from the x-ray diffraction and resistivity measurements, and it is shown in Fig. 9. The bar indicates the two-phase region in Fig. 7. The closed and open circles were obtained from resistivity measurements on heating and cooling, respectively. The triangles represent the midpoint of the transitions as observed by x-ray measurements (Fig. 5). The metal-insulator boundary is not well determined by resistivity measurements, as can be seen by comparing Figs. 5 and 8. A small percentage of the metal phase results in a large drop in the resistivity. Also, as the M-I phase boundary is a strong function of concentration, any concentration gradients or variations in strain in a crystal would smear out the observed transition. In contrast to this the M-I and I-AF phase boundaries are not as strongly dependent on concentration and on strain and these transitions are much sharper. Presumably a hypothetical uniform, unstrained crystal would show a sharp M-I transition. A decrease in resistivity suggesting an I-M transition in at least part of the sample was observed on cooling in samples with x as high as 0.02. Reasonable average curves were drawn through the data points to suggest the phase boundaries. The spread in the different points indicates the size of the hysteresis that is actually observed. The results of Fig. 9 are in good agreement with the M-I surface determined in studies of the solid-solid critical line as a function of pressure and temperature,[21] and also with magnetic susceptibility measurements made on the same samples.[22]

B. High-Pressure Experiments

These experiments were performed to establish an I-M transition as a function of pressure and to determine the pressure-temperature phase diagram of $(V_{0.96}Cr_{0.04})_2O_3$. Preliminary experiments using a standard Bridgman anvil geometry confirmed the existence of sharp transitions in the resistivity of over two orders of magnitude in samples with $x = 0.02$ and 0.04. Measurements were then made on the sample with $x = 0.04$. A girdle die with a ~ 0.4-cm^3 sample volume was used to produce pressures up to ≈ 50 kbar in conjunction with a cryostat capable of transmitting applied loads of 300 tons to a chamber at 4.2 °K.[7,41] The M-AF transition in pure V_2O_3 is very anisotropic in its stress dependence with $dT/dS_a = -6.8$ K/kbar and $dT/dS_c = -0.5$ K/kbar, where S_a and S_c are uniaxial stresses along the $\vec{a}$ and $\vec{c}$ hexagonal axis of the corundum structure.[33] In order to estimate the size of spurious effects which might be caused by the quasihydrostatic high-pressure apparatus, two crystals were mounted in the cell; one with the $\vec{c}$ axis parallel with the axis of applied load and one with the $\vec{c}$ axis perpendicular to the load. Pressure contacts were made to the samples with platinum ribbons so as to form a series circuit with the constant current supply and the voltage drop between the Pt ribbons measured by separate sets of voltage leads. In the resulting geometry the resistivity perpendicular to the $\vec{c}$ axis was measured in the crystal with the $\vec{c}$ axis parallel to the axis of applied load and vice versa for the other crystal. Disks of the AgCl pressure transmitting medium were cut out to just fit the sample and lead assembly. Finally, a Bi wire was mounted axially in the center of the cell between the two crystals but insulated from them. A two-lead resistance measurement was made between the anvils which contacted the Bi in order to calibrate the apparatus. A linear relation was assumed between applied load and pressure using the Bi I-II transition at 25.4 kbar as a fixed calibration point.

The experiment was carried out in five steps. First, the resistivity was measured as a function of increasing pressure at room temperature up through the I-M transition as shown in Fig. 10. Second, the resistivity as a function of temperature was measured from 77 to 298 °K at 13 kbar (above

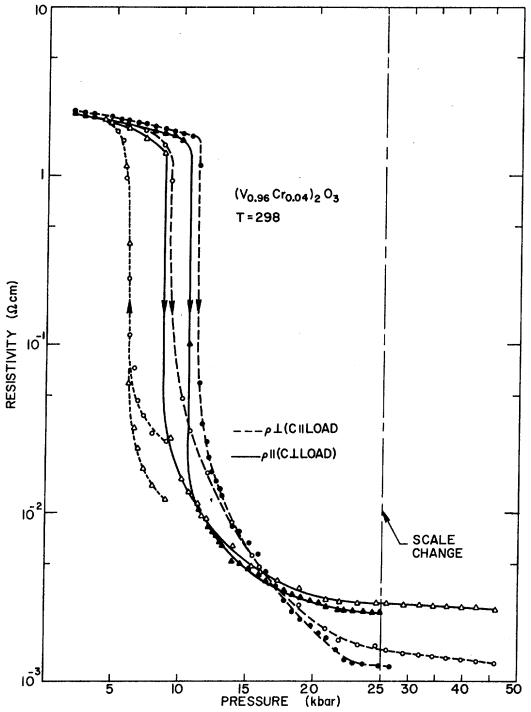

FIG. 10. Resistivity versus pressure at room temperature for $(V_{0.96}Cr_{0.04})_2O_3$. Dashed curves are for crystals with the c axis parallel to the axis of applied load and $\rho_\perp$ was measured. Solid curves are for a second crystal with c perpendicular to load and $\rho_{||}$. Closed symbols are for first cycle with increasing pressure. Open symbols are for a complete cycle through the transition after repeated cycling through M-AF transition and they show the general reproducibility of the I-M transition.

the I-M transition) and these results are compared with those obtained at 1 atm in Fig. 11. Third, after warming to room temperature the pressure was increased through the Bi I-II calibration point and then the M-AF phase boundary was determined by cycling through the transition with increasing and decreasing pressure while slowly cooling from 77 to 4.2 °K. The boundary was retraced while warming and all the results are shown in Fig. 12. The quasihydrostatic nature of the pressure transmitting medium is evident at low temperatures where the AF-M transition occurs at a higher pressure for the crystal with the less stress sensitive $\vec{c}$ axis parallel to the axis of applied load. The critical pressure for the suppression of the AF phase is 41 ± 6 kbar. For comparison, the dashed curve is the average M-AF phase boundary for pure V_2O_3.[42] In the fourth step the reproducibility of the I-M transition at room temperature, after repeated cycling through M-AF transition, was established and the results are compared with the initial cycle in Fig. 10. The assumption of a linear relation between applied load and pressure becomes questionable at low pressures and this may account for part of the observed 3–4-kbar hysteresis. The I-M transition is slightly broader and appears to be shifted to lower pressures (~ 10%) by the previous treatment. In the final step the resistivity was measured up to 47 kbar (Fig. 10), and the metallic nature of the samples at these pressures confirmed by measuring the resistivity from 4.2 to 298 °K as shown in the inset of Fig. 12. It must be empha-

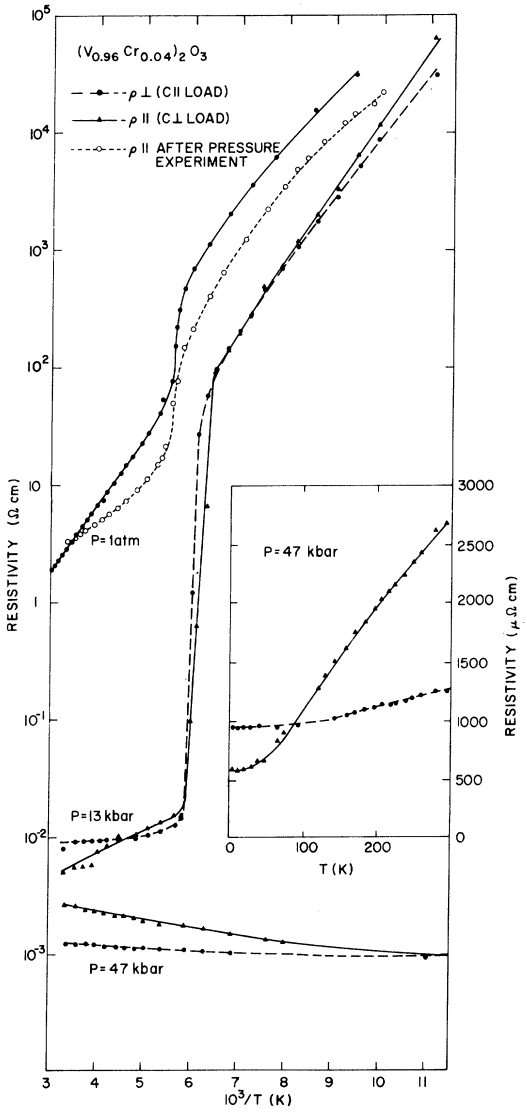

FIG. 11. Resistivity versus reciprocal temperature at different pressures for $(V_{0.96}Cr_{0.04})_2O_3$. The symbols are the same as Fig. 10. The dotted curve with open circles was obtained at 1 atm after unloading the high-pressure apparatus, and it shows the deterioration of the sample from cycling through the transitions and from the quasihydrostatic nature of the pressure. The inset shows the resistivity versus temperature above the critical pressure for the suppression of AF phase.

sized that these results were obtained on crystals that are severely strained and cracked from cycling through the M-AF transition, and that a true four-probe method was not used (i.e., contact resistance between sample and Pt foil is included). Consequently, they are only meant to show the qualitative features of the resistivity above the critical pressure and are not to be compared with earlier measurements on pure V_2O_3 which were done on fresh crystals using a four-probe method.[42] More extensive measurements of the transport properties are planned.

A few preliminary measurements were made to establish the existence of an I-M transition at higher Cr concentrations. The size of the crystals with $x = 0.12$ was very small and, therefore, a Bridgman anvil geometry was used. Five to ten small crystals were placed in a hole in the AgCl disk between two Pt foils which in turn contacted the 1.27-cm faces of the anvils. A two-lead resistance measurement was made across the anvils. An Isomica gasket was used to contain the AgCl. In this geometry only sharp changes in the sample resistivity can be detected and no attempt is made to assign an absolute resistivity. As shown in Fig. 13, an anomaly does occur at high pressures for a sample with $x = 0.12$. No anomaly was observed under the same conditions for pure V_2O_3. A rough estimate of the pressure was made by running a Bi wire in the same geometry, and the pressure at which the anomaly occurs in $(V_{0.88}Cr_{0.12})_2O_3$ is estimated to be 34 ± 5 kbar.

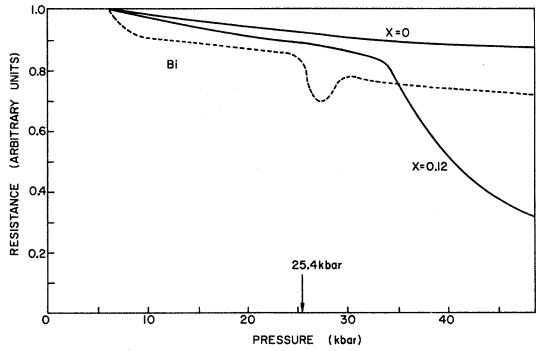

FIG. 13. Approximate resistance-versus-pressure curves at room temperature using Bridgman anvils. Comparison of sample with $x = 0.12$ with pure V_2O_3 ($x = 0.0$) shows transition at ≈ 34 kbar relative to Bi in $x = 0.12$ sample. Resistance normalized to 1 at ≈ 6 kbar.

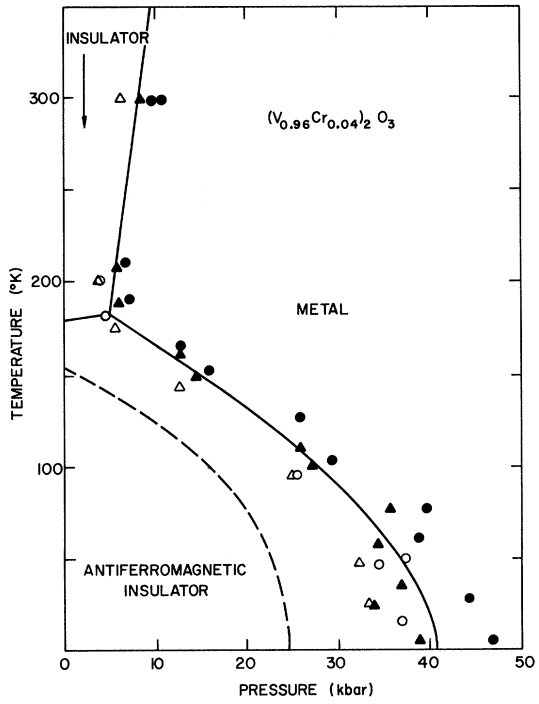

FIG. 12. Temperature-pressure phase diagram for $(V_{0.96}Cr_{0.04})_2O_3$. Symbols are same as Fig. 10 and an average curve has been drawn through the data points for simplicity. The dashed curve is the M-AF boundary for pure V_2O_3 after Ref. 38.

IV. DISCUSSION

In this section the different transition-metal oxides are compared, and it is shown that M-I transitions appear to occur in the monoxides, the sesquioxides, and the dioxides with increasing atomic number. A pressure-temperature-composition diagram for $(V_{1-x}Cr_x)_2O_3$ is constructed, and it is shown that the lattice and various physical properties are affected as the transition region is approached. A comparison of the transitions in V_2O_3 and VO_2 reveals striking differences. A detailed comparison of the results with the various microscopic theories has been presented elsewhere.[20]

In Fig. 14 the trend in electrical properties is summarized for (a) the MO compounds with the NaCl structure, (b) the M_2O_3 compounds with the α-corundum structure, and (c) the MO_2 compounds with the rutile structure. In many cases the structures are slightly distorted as indicated by the shading of the boxes. The trend in electrical properties is also indicated by the shading. The electrical resistivity at room temperature is given in the upper right of each box, but only order-of-magnitude values are quoted, since the resistivity is very insensitive to impurities. The different temperature-induced transitions found in the oxides are summarized in the bottom of each box with the type of transition on the left and the transition temperature on the right.

In the monoxides there is a change from metallic to insulating behavior with increasing atomic number.[43] All those to the right in Fig. 14 are antiferromagnetic insulators, whereas on the left they

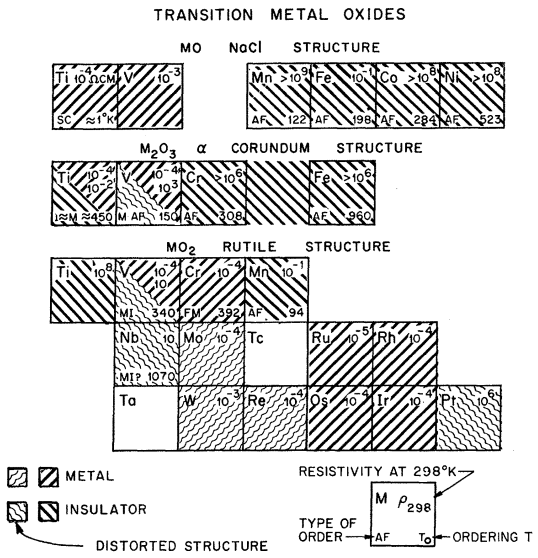

FIG. 14. Comparison of electrical properties of different transition-metal oxides. Data obtained from Refs. 4, 13, 45, and D. B. Rogers, R. D. Shannon, A. W. Sleight, and J. L. Gillson [Inorg. Chem. 8, 841 (1969)]. SC – superconducting, I≈ M – continuous insulator-metal transition, M-I – sharp metal-insulator transition, M-AF – metal-antiferromagnetic-insulator transition, AF – paramagnetic antiferromagnetic, and FM – paramagnetic-ferromagnetic transition. (The resistivity of each phase is given for oxides with M-I and M-AF transitions.)

are metallic with TiO being a superconductor.[28] At one time it was thought that VO had a temperature-induced metal-insulator transition, but recent studies have failed to find this transition in well-characterized material.[28,44] In fact, VO changes continuously from a metal for $V_{1+x}O$ to a semiconductor for VO_{1+x}.

Turning to the sesquioxides, there is a region of metallic behavior at the beginning of the series. Ti_2O_3 is a semiconductor at low temperatures and changes to metallic behavior in the 400–500 °K range.[45] This is not a transition in the thermodynamic sense. Rather, a model involving continuous changes in band structure has been proposed to explain the observed properties.[46] The addition of a few percent of V_2O_3 to Ti_2O_3 produces metallic behavior at room temperature which persists to pure V_2O_3.[18,47] The present work shows that a first-order M-I transition occurs at room temperature at $x = 0.01$ in $(V_{1-x}Cr_x)_2O_3$. Since the M-I and M-AF transitions occur both as a function of Cr concentration and pressure, they should be represented by surfaces in a temperature-pressure-composition phase diagram. Combining the curves in Figs. 9 and 12, a three-dimensional diagram was constructed as shown in Fig. 15. If the M-I surface is extrapolated to pure V_2O_3, an M→I transition should be expected at 500–600 °K. In fact, the resistivity does show a region of anomalous increase in the direction of approaching the resistivity observed in insulating samples (Fig. 9). The lattice parameters also show regions of anomalous change in the direction of approaching the parameters of insulating $(V_{0.96}Cr_{0.04})_2O_3$ (Fig. 4). Finally, the magnetic susceptibility shows an anomaly as a function of temperature, and it is indistinguishable from the susceptibility of $(V_{0.96}Cr_{0.04})_2O_3$ above this temperature region.[22] The change from metallic to more insulating behavior is continuous and is not a transition in the thermodynamic sense. On the other hand, a first-order transition is observed (i) as a function of temperature in $(V_{0.99}Cr_{0.01})_2O_3$ (Figs. 5 and 9), (ii) as a function of pressure in $(V_{0.96}Cr_{0.04})_2O_3$ (Figs. 6 and 10), and (iii) as a function of composition (Figs. 1 and 7). This suggested that the first-order M-I transition for a given Cr concentration might terminate in a solid-solid critical point[20] similar to that observed in Ce metal.[48] Experiments on several mixed oxides as a function of temperature and pressure have given strong evidence for a critical line as a function of Cr concentration, and the M-I surface in Fig. 15 terminates at the experimentally determined line.[21] Extrapolation to pure V_2O_3 gives a critical point at −1.6 kbar and 474 °K and is in agreement with a continuous M-I transition at 1 atm around 500–600 °K.

It is worth speculating on the extension of the phase diagram to higher Cr concentrations and also to mixed oxides containing Ti. The I-M critical temperature decreases with increasing Cr concen-

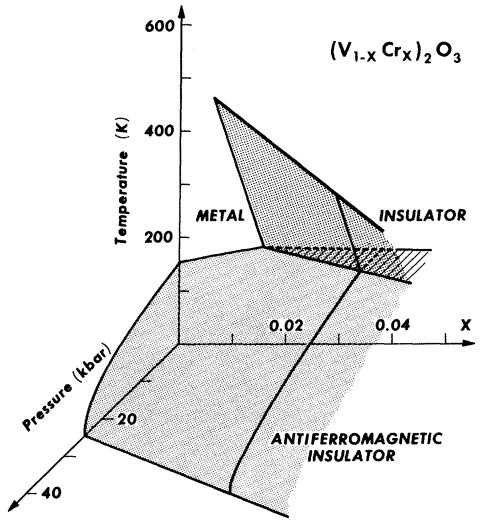

FIG. 15. Temperature-pressure-composition phase diagram showing M-I, M-AF, and I-AF surfaces. M-I surface terminates at a solid-solid critical line after Ref. 21. Other boundaries are from Figs. 9 and 11 and Ref. 42.

tration and, assuming a linear dependence on x, the predicted critical temperature for $x = 0.12$ is ≈ 200 °K.[21] At 300 °K, a rather broad transition was found at ≈ 34 kbar in $(V_{0.88}Cr_{0.12})_2O_3$ so the critical temperature may decrease more slowly with increasing Cr concentration. As a sharp I-M transition occurs at the V-rich end of $(V_{1-x}Cr_x)_2O_3$ as a function of pressure, it is reasonable to expect a similar transition at the Cr-rich end but at a much higher pressure. Another I-M surface should then exist as a function of V_2O_3 in Cr_2O_3. It is not clear at what pressure and composition the surfaces from the Cr-rich and the V-rich ends would intersect. It may be that near the middle of the $(V_{1-x}Cr_x)_2O_3$ system the atomic disorder broadens the I-M transition into a continuous rather than a first-order transition. In this case the two surfaces will not meet. At low temperatures it is difficult to predict the transitions in the pressure-composition plane. At 1 atm both V_2O_3 and Cr_2O_3 are antiferromagnetic, but they have different crystal structures. The transition from one structure to the other appears to be near $x \approx 0.25$–0.30,[22] but an intermediate phase with a different spin structure may exist as in the Cr_2O_3–Fe_2O_3 system.[49]

Figure 15 suggests that the area in the T-P plane enclosed by the M-AF boundary is decreasing with decreasing Cr concentration. This leads to the speculation that the antiferromagnetic insulating phase will be completely suppressed in the $(V_{1-x}Ti_x)_2O_3$. Measurements of the electrical resistivity on ceramic material support this idea.[18,47] We have not yet grown crystals of these mixed oxides in order to establish the details of the suppression of the AF phase.

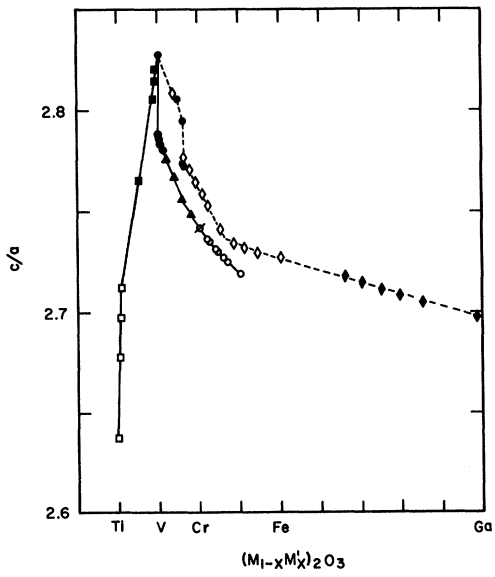

FIG. 16. c/a ratio for pure and mixed sesquioxides $(M_{1-x}M'_x)_2O_3$: circles, this work; open squares, Ref. 47; squares, Ref. 18; triangles, Ref. 17; open circles, Ref. 49; open diamonds, Ref. 50; and diamonds, Ref. 51.

The general picture that emerges from this work is that a boundary does exist between the two classes of materials, i.e., those described using a band or a localized approach. This transition is not, however, from a good metal to a good insulator. The properties on each side of the critical composition or pressure are affected by the impending transition. This is clearly seen in the c/a ratio of the lattice parameters. The c/a ratios for pure and mixed oxides of the form $(M_{1-x}M'_x)_2O_3$, where M-M' are Ti-V,[18,47] V-Cr,[17] Cr-Fe,[49] V-Fe,[50] and Fe-Ga,[51] are plotted against the average atomic number of M and M' in Fig. 16. A sharp peak occurs at V_2O_3 and an equally dramatic drop occurs at Ti_2O_3. Starting at the right in Fig. 16, there is a gradual rise in c/a ratio with decreasing average M. There is a clear change in slope between Fe_2O_3 and Cr_2O_3, and the c/a ratio increases much more rapidly until the discontinuity at the transition to the metallic state is reached. The discontinuity occurs at a lower vanadium concentration in the V-Fe system than in the V-Cr system.

The increase in the c/a ratio as the metallic state is approached is also seen in the x-ray measurements at high pressure. At the insulator-metal transition in $(V_{0.96}Cr_{0.04})_2O_3$, Fig. 6 shows that c/a increases sharply. Also with increasing pressure V_2O_3 becomes more metallic and the antiferromagnetic-insulating phase is completely suppressed above 26 kbar. The x-ray measurements show that c/a increases with increasing pressure in V_2O_3. In contrast, in materials which are not near the critical region, c/a is much less pressure or volume sensitive; $d\ln(c/a)/d\ln V = -0.7$ (V_2O_3), -0.3 (Ti_2O_3), -0.3(Cr_2O_3), 0.0(Fe_2O_3), and $+0.1$(Al_2O_3).[34] An increase in c/a accompanied by an increase in metallic character is also observed in Ti_2O_3 at 1 atm with increasing temperature.[52]

These changes in c/a indirectly reflect changes in interatomic distances in the crystals. Refinements of the crystal structures of the corundum phase of V_2O_3 and $(V_{0.96}Cr_{0.04})_2O_3$[53] and of the monoclinic phase of V_2O_3[25] have shown that the V – V distances in the metallic phase are shorter or equal to the distances in both insulating phases. (A previous speculation that vanadium atoms paired in the basal plane at the M → AF transition is not supported by the recent crystal structure refinements.[25,54]) The nature of the changes in interatomic distances on going from V_2O_3 to $(V_{0.96}Cr_{0.04})_2O_3$ at room temperature is shown schematically in Fig. 2. The V – V distance parallel to the $\vec{c}$ axis (across the face of the oxygen octahedra) increases but the V – O distances remain almost unchanged.[53] This results in an expansion of the triangles of oxy-

gen atoms on the top and bottom of the face-shared octahedra and a contraction of the triangle in the middle (see Fig. 3). This in turn results in the expansion in $\vec{a}$ and the contraction in $\vec{c}$ which is observed in Fig. 1.

In addition to the lattice, many physical properties show marked changes both at the transition and over a wide range of concentration and pressure near the critical region. All the experimental evidence points to a system with strong interactions, whence reliable theoretical calculations of different physical properties in this region are very difficult to perform. Metallic V_2O_3 lies very near to the critical region for the Mott transition and some of its physical properties are summarized in Table I. It is clear that most of the properties are highly anomalous. All the volume derivatives are large showing that with decreasing pressure V_2O_3 becomes a poorer and poorer metal as the critical region is approached. Physically it seems reasonable to expect that as the critical region is approached both the metallic and the insulating states would exhibit fluctuations toward the other state. On the metallic side this might take the form of spin fluctuations[19,20] or on the insulating side the virtual formation of V^{2+}-V^{4+} pairs. It has also been emphasized by Mott that V_2O_3 is a polar crystal and that electron-phonon interactions might greatly modify the nature of the transition.[55]

Returning to Fig. 14, a comparison should be made of the transition in $(V_{1-x}Cr_x)_2O_3$ with those in the dioxides. VO_2 is one of the few materials reported in the literature which has as dramatic a temperature induced M-I transition as V_2O_3. There are many materials which show changes in the resistivity of one or two orders of magnitude,[12] but only V_2O_3 and VO_2 and perhaps some of the Magneli phases have sharp changes of $>10^5$. The entropy changes at the transition in V_2O_3 and VO_2 are also similar, but there are also striking differences. The transition in V_2O_3 is to an antiferromagnetic phase which, as shown in Fig. 16, is associated with the M-I transition and the ordering of the resulting local moments in the insulating phase. The low-temperature phase of VO_2 is not magnetically ordered, but there is a lattice distortion associated with the transition.[56] However, the crystal structure of the insulating phase of VO_2 is the same as that of the metallic oxides MoO_2, WO_2, and ReO_2.[57] Figure 14 suggests that the type of M-I transition which occurs in the $(V_{1-x}Cr_x)_2O_3$ system will occur in the dioxides in the $Mn_{1-x}Cr_xO_2$ system. In fact, an anomaly does occur in the c/a ratio of MnO_2 with increasing pressure.[34] Also a two-phase region of rutile structures of different densities has been reported in this system,[58] but the Mn-rich phase was more dense which is surprising. It should be mentioned that the control of oxidation states in these systems is difficult.

Distortions of the rutile structure occur in several dioxides (see Fig. 14); however, the mixed oxides show extended regions where the undistorted rutile structure is stable.[57] This suggests that the interaction that causes the distortions is destroyed by the disorder in the mixed oxides.

The crystal chemistry of VO_2 is anomalous among the dioxides since there are two monoclinic distortions. At room temperature the addition of impurities of the form $V_{1-x}M_xO_2$, where M = Ti, Cr, or W, results in a transition from one monoclinic distortion to another and then to undistorted rutile with increasing x.[59] There is also evidence for an intermediate distorted phase in VO_2 between the monoclinic and the rutile phases as a function of temperature.[60,61] At present, the different phase boundaries have not been studied in detail, but it appears that the large change in resistivity accompanies the transition from the rutile phase to the intermediate monoclinic phase in VO_2.[62] As the temperature range over which the intermediate phase is stable decreases with decreasing impurity content, pure VO_2 may show a single transition.

The monoclinic phase stable at room temperature is derived from the tetragonal rutile structure by $\vec{a} = 2\vec{c}_R$, $\vec{b} = \vec{a}_R$, and $\vec{c} = \vec{a}_R + \vec{c}_R$ and involves a pairing of V atoms along the $\vec{c}_R$ direction. The intermediate phase involves a distortion of the lattice in the basal plane of the rutile structure and not along

TABLE I. Properties of metallic V_2O_3.

Resistivity ($\mu\Omega$ cm):		
1 atm:	$\rho = 227 \pm 1.4T$	$(150 < T < 350)$ [a]
26 kbar:	$\rho = 182 \pm 0.7T$	$(200 < T < 300)$ [b]
	$\rho = 31 \pm 0.042T^2$	$(T < 50)$. [b]
$d\ln\rho/d\ln V = 30$ (basal plane) and 16 ($\parallel c$ axis). [a]		
Hall coefficient $R_H = 2.3 \times 10^{-4}$ cm^3/C (p type) [c]; no change in R_H at anomaly at 500–600 °K.		
Seebeck coefficient 12 μ^v/°C. [c]		
Magnetic susceptibility [d] (cgs/mole):		
	$\chi = 2.1 \times 10^{-4} + 1.40/(T+600)$	$(180 < T < 350)$
	$\chi = 2.1 \times 10^{-4} + 1.78/(T+600)$	$(580 < T < 1000)$.
Knight shift [e,f] (%):		
	$k = +1.52 - 18.1/(T+684)$;	
no change in k at 500–600 °K anomaly:		
	$k = (-1.0 \pm 0.2) + (0.01 \pm 0.005)P$	
	$(26 < P < 65$ kbar and $T = 4.2$ °K).	

[a] Reference 33 value is smaller than given in Ref. 42 because experimental value of bulk modulus is used.
[b] Reference 42.
[c] Austin and Turner [Phil. Mag. 19, 939 (1969)].
[d] Reference 22.
[e] Reference 16.
[f] Reference 23.

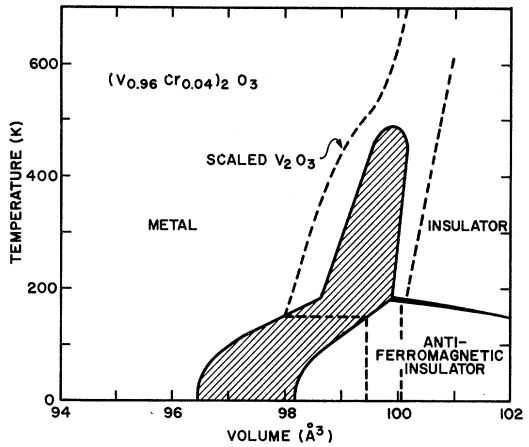

FIG. 17. Temperature-volume phase diagram for $(V_{0.96}Cr_{0.04})_2O_3$. Shaded area is the volume excluded at the different transitions. Dashed curves are thermal expansion at 1 atm of 4%-Cr sample and pure V_2O_3. The latter is plotted as if it were the 4% sample under a pressure of ≈ 13.5 kbar after Ref. 19.

$\vec{c}_R$. Choosing the unique monoclinic axis as $\vec{c}$, then $\vec{a}_M \approx \vec{b}_M \approx \vec{a}_R$ and $\vec{c}_M \approx \vec{c}_R$ and the monoclinic angle γ is slightly larger than 90° (90.3°–90.6°).[59] This suggests that the traditional interpretation of the transition in VO_2 must be modified to account for the occurrence of one monoclinic phase nested in another one.

At present there does not appear to be a definitive microscopic theory of the Mott transition. It is not clear why V_2O_3 and VO_2 appear to have different mechanisms for their respective transitions. Also, the Mott transition has been observed with the addition of Al_2O_3, Sc_2O_3, and Fe_2O_3 to V_2O_3 as well as Cr_2O_3.[18,63] It is not clear why these ions cause an expansion of the lattice and an M→I transition.

ACKNOWLEDGMENTS

The authors thank A. M. Clogston and T. M. Rice for their continued interest and help in this problem. We also thank K. Andres, A. C. Gossard, A. Jayaraman, M. Marezio, A. Menth, and W. M. Walsh, Jr., for helpful discussions. We thank A. S. Cooper, P. D. Dernier, E. Kelly, and A. L. Stevens for technical assistance.

APPENDIX: TEMPERATURE-VOLUME-PHASE DIAGRAM FOR $(V_{0.96}Cr_{0.04})_2O_3$

Theoretical calculations are usually done as a function of volume rather than pressure. An approximate temperature-volume phase diagram can be constructed from the temperature-pressure phase diagram for $(V_{0.96}Cr_{0.04})_2O_3$. The volume at 1 atm as a function of temperature [Fig. 5(a)] is used as a starting line. Assuming a Birch equation with $B_0 = 2140$ and assuming that B_0 is independent of temperature, the transition pressures in Fig. 12 can be converted to changes in volume. This establishes half of the phase diagram. In order to estimate the excluded volume at the transition, the observed volume change at the M-I transition at 1 atm as a function of Cr concentration is used.[21] This is extrapolated to zero at the experimentally determined critical temperature and also extrapolated smoothly to $T = 0$.[21] The volume change at the M-AF transition in V_2O_3 is found to be within 0.2% of this curve. The resulting phase diagram is shown in Fig. 17. It was shown that the effect of increasing pressure and decreasing Cr could be scaled with a factor of 3.6-kbar/% Cr.[19] Using this factor the volume-versus-temperature curve for V_2O_3 at 1 atm can be plotted as if it were $(V_{0.96}Cr_{0.04})_2O_3$ under a pressure of ≈ 13.5 kbar. One notes that the high-temperature anomaly does follow the phase boundary and bears a striking similarity to supercritical behavior in a liquid-gas system. Also, although at a constant pressure the sequence AF-M-I can be observed for certain concentrations, this is not observed at constant volume.

[1]J. H. deBoer and E. J. W. Verwey, Proc. Phys. Soc. (London) 49, 59 (1937); R. Peierls, *ibid.* 49, 72 (1937).
[2]N. F. Mott, Proc. Phys. Soc. (London) 62, 416 (1949).
[3]N. F. Mott, Phil. Mag. 6, 287 (1961).
[4]Rev. Mod. Phys. 40, (1968), entire issue.
[5]H. G. Drickamer, Solid State Phys. 17, 1 (1965).
[6]For an account of the excitonic phase transition, see B. I. Halperin and T. M. Rice, Solid State Phys. 21, 115 (1968) and references therein; W. Kohn, in *Many-Body Physics*, edited by C. DeWitt and R. Balian (Gordon and Breach, New York, 1968), p. 351.
[7]D. B. McWhan, T. M. Rice, and P. H. Schmidt, Phys. Rev. 177, 1063 (1969).
[8]D. Jerome, Solid State Commun. 7, 957 (1969).
[9]S. Minomura and H. G. Drickamer, J. Appl. Phys. 34, 3043 (1963).
[10]M. Föex, Compt. Rend. 223, 1126 (1946); J. Rech. Centre Natl. Rech. Sci. Lab. Bellevue (Paris) 4, 238 (1951).
[11]J. Jaffray and D. Dumas, J. Rech. Centre Natl. Rech. Sci. Lab. Bellevue (Paris) 5, 360 (1954).
[12]F. J. Morin, Phys. Rev. Letters 3, 34 (1959).
[13]For a review of work on V_2O_3, see D. Adler, Solid State Phys. 21, 1 (1968).
[14]R. M. Moon, J. Appl. Phys. 41, 883 (1970).
[15]K. Kosuge, J. Phys. Chem. Solids 28, 1613 (1967).
[16]E. D. Jones, Phys. Rev. 137, A978 (1965).
[17]R. E. Newnham and Y. M. de Haan, Laboratory for Insulation Research, Massachusetts Institute of Technology Progress Report No. 26, 1960 (unpublished).
[18]A. J. MacMillan, Laboratory for Insulation Research, Massachusetts Institute of Technology Report No. 172, 1962 (unpublished).

[19]D. B. McWhan, T. M. Rice, and J. P. Remeika, Phys. Rev. Letters 23, 1384 (1969).
[20]T. M. Rice and D. B. McWhan, IBM J. Res. Develop. 14, 251 (1970).
[21]A. Jayaraman, D. B. McWhan, J. P. Remeika, and P. D. Dernier, Paper II in this series, Phys. Rev. B 2, 3751 (1970).
[22]A. Menth and J. P. Remeika, Paper III in this series, Phys. Rev. B 2, 3756 (1970).
[23]A. C. Gossard, D. B. McWhan, and J. P. Remeika, Paper IV in this series, Phys. Rev. B 2, 3762 (1970).
[24]K. Andres, Paper V in this series, Phys. Rev. B 2, 3768 (1970).
[25]P. D. Dernier and M. Marezio, Paper VI in this series, Phys. Rev. B 2, 3771 (1970).
[26]W. F. Brinkman and T. M. Rice, Phys. Rev. B 2, 1324 (1970).
[27]A. C. Gossard (private communication).
[28]M. D. Banus and T. B. Reed, in *The Chemistry of Extended Defects in Non-Metallic Solids*, edited by L. Eyring and M. O'Keefe (North-Holland, Amsterdam, 1970), p. 488.
[29]E. P. Warekois, J. Appl. Phys. Suppl. 31, 346 (1960).
[30]S. C. Abrahams, Phys. Rev. 130, 2230 (1963).
[31]*International Tables for X-ray Crystallography* (Kynoch Press, Birmingham, 1952).
[32]S. Minomura and H. Nagaraki, J. Phys. Soc. Japan 19, 131 (1964).
[33]J. Feinleib and W. Paul, Phys. Rev. 155, 841 (1967).
[34]H. G. Drickamer, R. W. Lynch, R. L. Clendenen, and E. A. Perez-Albuerne, Solid State Phys. 19, 135 (1966).
[35]D. B. McWhan and W. L. Bond, Rev. Sci. Instr. 35, 626 (1964).
[36]J. C. Jamieson and B. Olinger, Proceedings of the Conference on Accurate Characterization of the High Pressure Environment, National Bureau of Standards, Gaithersburg, Maryland, 1968 (unpublished).
[37]D. B. McWhan, Trans. Am. Cryst. Assoc. 5, 39 (1969).
[38]F. Birch, J. Geophys. Res. 57, 227 (1952).
[39]E. Schreiber and O. L. Anderson, J. Am. Ceram. Soc. 49, 184 (1966).
[40]R. C. Liebermann and E. Schreiber, J. Geophys. Res. 73, 6585 (1968).
[41]D. N. Lyon, D. B. McWhan, and A. L. Stevens, Rev. Sci. Instr. 38, 1234 (1967).
[42]D. B. McWhan and T. M. Rice, Phys. Rev. Letters 22, 887 (1969).
[43]J. Goodenough, Czech. J. Phys. B17, 304 (1967).
[44]W. W. Warren, Jr., A. C. Gossard, and M. D. Banus, J. Appl. Phys. 41, 881 (1970).
[45]J. M. Honig and T. B. Reed, Phys. Rev. 174, 1020 (1968), and references therein.
[46]L. L. VanZandt, J. M. Honig, and J. B. Goodenough, J. Appl. Phys. 39, 594 (1968).
[47]T. Kanakubo, T. Yanagi, and S. Nomura, J. Phys. Soc. Japan 15, 2102 (1960).
[48]A. Jayaraman, Phys. Rev. 137, A179 (1965).
[49]D. E. Cox, W. J. Takei, and G. Shirane, J. Phys. Chem. Solids 24, 405 (1963).
[50]D. E. Cox, W. J. Takei, R. C. Miller, and G. Shirane, J. Phys. Chem. Solids 23, 863 (1962).
[51]C. T. Prewitt, R. D. Shannon, D. B. Rogers, and A. W. Sleight, Inorg. Chem. 8, 1985 (1969).
[52]A. D. Pearson, J. Phys. Chem. Solids 5, 316 (1958).
[53]P. D. Dernier, J. Phys. Chem. Solids (to be published).
[54]J. Goodenough, *Magnetism and the Chemical Bond* (Interscience, New York, 1963).
[55]N. F. Mott, Phil. Mag. 20, 1 (1969).
[56]For a review of the properties of VO_2, see C. N. Berglund and H. J. Guggenheim, Phys. Rev. 185, 1022 (1969).
[57]B. O. Marinder and A. Magneli, Acta Chem. Scand. 12, 1345 (1958).
[58]K. Siratori and S. Iida, J. Phys. Soc. Japan 15, 210 (1960).
[59]M. Israelsson and L. Kihlborg, Mater. Res. Bull. 5, 19 (1970); J. Galy, A. Casalot, J. Darriet, and P. Hagenmuller, Bull. Soc. Chim. France 227 (1967).
[60]T. Mitsuishi, Japan. J. Appl. Phys. 6, 1060 (1967).
[61]M. Nygren and M. Israelsson, Mater. Res. Bull. 4, 881 (1969).
[62]An anomaly in the resistivity of VO_2 is observed with increasing temperature in the insulating phase before the transition to the metallic phase. See J. B. MacChesney and H. J. Guggenheim, J. Phys. Chem. Solids 30, 225 (1969).
[63]D. B. McWhan and J. P. Remeika (unpublished).